Crystallographic features of the orbital-ordered, and charge-and-orbital-ordered states in $Sr_{2-x}Nd_xMnO_4$

Wataru Norimatsu* and Yasumasa Koyama
Department of Photonic and Electronic Systems, School of Fundamental Science and Engineering, Waseda University, Shinjuku-ku, Tokyo 169-8555, Japan
and Kagami Memorial Laboratory for Materials Science and Technology, Waseda University, Shinjuku-ku, Tokyo 169-0051, Japan
(Received 25 December 2006; revised manuscript received 9 April 2007; published 25 June 2007)

The crystallographic features of the orbital-ordered and charge-and-orbital-ordered states in $Sr_{2-x}Nd_xMnO_4$ have been investigated by *in situ* observations, using a transmission electron microscope, in an attempt to understand the distinct characteristics of their electronic states. In the orbital-ordered state with orthorhombic symmetry, there exist four banded-domain-structure states, that is, two orthorhombic variant states (O_I+O_{II}) accompanying the *C*-type antiferromagnetic ordering at lower temperatures and (DT+O_I) coexistence and (O_I+O_{II}) states lacking magnetic ordering at higher temperatures, where DT represents the disordered tetragonal state and O_I and O_{II} the two orthorhombic variants. On the other hand, the stability of the charge-and-orbital-ordered state present for $0.25 \leqslant x \leqslant 0.43$ is strongly suppressed when $x > 0.38$. As a result of the strong suppression, the charge-exchange-type charge-and-orbital-ordered state is absent for $x=0.5$. The important features of the charge-and-orbital-ordered state are that it is basically characterized by incommensurate structural modulations and that round-shaped domains separated by disordered regions appear for $0.38 < x \leqslant 0.43$ near the DT state. On the basis of these data, the origin of the appearance of the four banded-structure states in the orbital-ordered state was attributed to a coupling between the local Jahn-Teller distortion and the long-range distortions, including a dilational one. In addition, we propose a model for the ground-state change between the orbital-ordered and charge-and-orbital-ordered states in terms of orbital degree of freedom.

DOI: 10.1103/PhysRevB.75.235121 PACS number(s): 71.38.−k, 75.47.Lx, 68.18.Jk, 68.37.Lp

I. INTRODUCTION

The colossal magnetoresistance (CMR) in manganites, observed as the drastic reduction of resistivity in a magnetic field, is one of the fascinating phenomena found in strongly correlated electron compounds.[1–3] The CMR effect is understood to be directly associated with the coexistence of the ferromagnetic metallic and antiferromagnetic insulating phases, an occurrence of which has been explained on the basis of several models, such as the random-interaction model and the two-type-distortion model.[4–8] However, in spite of these proposals, the origin of the effect in strongly correlated manganites is still of central interest.

The $Sr_{2-x}Nd_xMnO_4$ (SNMO) system is one of the layered perovskite manganites with the K_2NiF_4-type structure.[9–11] This structure is characterized by the presence of a single MnO_2 layer separating two neighboring NaCl-type block layers. The single MnO_2 layer thus provides, basically, a two-dimensional electronic system. In such a SNMO, the end-oxide insulator Sr_2MnO_4 has an electronic configuration of t_{2g}^3 for Mn^{4+} ions and exhibits a two-dimensional antiferromagnetic behavior.[12] When the Sr^{2+} ions are partially replaced by Nd^{3+} ions, e_g electrons are doped into the system via the introduction of Mn^{3+} ions. Our preliminary work on SNMO with $0.10 \leqslant x \leqslant 0.50$, as a result, suggested the existence of an orbital-ordered (OO) state lacking charge ordering for $0.1 \leqslant x \leqslant 0.25$, an incommensurate charge-and-orbital-ordered (ICOO) state for $0.25 \leqslant x \leqslant 0.43$, and a disordered tetragonal (DT) state for $0.43 < x \leqslant 0.50$.[13] Among these states, the OO state with orthorhombic (*O*) symmetry is distinguished by both the e_g-electron occupation of the $(3x^2-r^2)$ or $(3y^2-r^2)$ orbital and the occurrence of *C*-type antiferromagnetic (CAF) ordering at lower temperatures. The points to note here are that the ICOO state in SNMO features incommensurate modulations that include higher-order commensurate ones and that the charge-exchange-type charge-and-orbital-ordered (CECOO) state is absent for $x=0.5$, unlike the case of $Sr_{2-x}La_xMnO_4$ (SLMO).[14–20] These facts indicate that the ICOO state probably has some relation to the OO state, rather than to the CECOO. Although the detailed electronic features of the ICOO state have so far been discussed in relation to the presence of the CECOO state, it seems to us that a reexamination of the crystallographic features of the ICOO state is needed to clarify its distinct characteristics.

Our previous *in situ* transmission electron microscopy (TEM) observations for the DT-to-OO transition in SLMO and SNMO revealed that the formation of the OO state during the cooling process from the DT state exhibited a unique domain-structure evolution.[13,19,20] The notable feature of the evolution is that the cooling from the DT state first results in a (DT+O_I) banded domain structure and then in a (O_I +O_{II}) banded structure in the OO state. Here, O_I and O_{II} represent two *O* variants with different b/a values, that is, each variant has a unique orthorhombicity. Among these results, the appearance of the (DT+O_I) banded structure obviously provides direct evidence for the coexistence of the DT and OO states. In other words, the coexistence of two states appears in the formation of the OO state, just as in the case of the CMR effect. As Ahn *et al.* have pointed out, this coexistence has been presumed to be due to a coupling between the short-range Jahn-Teller (JT) distortion and the

long-range distortion in the two-type-distortion model.[6,7] However, we believe that the essential origin of the coexistence in the K_2NiF_4-type manganites is still an open question.

In summary, then, the detailed features of the OO and ICOO states in SNMO appear to be insufficiently understood. In this situation, our interest is focused on SNMO, in particular, on a deeper understanding of both the OO state, including the (DT+OO) coexistence state, and the incommensurate modulations in the ICOO state. Thus, we have investigated, by transmission electron microscopy, the detailed crystallographic features of both the DT-to-OO and DT-to-ICOO transitions in SNMO samples with $0.10 \leqslant x \leqslant 0.50$ between room temperature and 15 K. Based on the collected experimental data, we discuss here the characteristic features of the OO state including the coexistence of the DT and OO states and propose a model for a ground-state change between the OO and ICOO states in terms of the orbital occupation of e_g electrons.

II. EXPERIMENTAL PROCEDURE

In the present experiment, most of the homogeneous SNMO samples with $0.10 \leqslant x \leqslant 0.50$ were prepared by a coprecipitation technique using citric acid, with $SrCO_3$, Nd_2O_3, and $MnCO_3$ initial powders. A number of SNMO samples made by a solid-state reaction were also used to check the reproducibility of the obtained experimental data. In the preparation, sample powders obtained by coprecipitation were first calcined at 1223 K for 12 h, and were then pressed into pellets. Sintering of sample pellets was carried out at 1773 K for 24 h in an O_2 atmosphere. The crystallographic features of the samples obtained were thus examined by transmission electron microscopy. The *in situ* observations were carried out between room temperature and 15 K, with a JEM-3010-type transmission electron microscope equipped with a liquid-He-cooling holder. An Ar-ion thinning method was used to prepare thin samples for observation. Note that, in this paper, crystallographic planes and directions and reflections in electron diffraction patterns were indexed in the pseudotetragonal notation.

III. EXPERIMENTAL RESULTS

An electronic phase diagram of the Nd-poor portion of SNMO, as determined by our preliminary and present investigations, is shown in Fig. 1, together with dark field images of the OO (CAF), ICOO, and DT states at 15 K.[13] The images in (b), (c), and (d) were taken, respectively, from samples with $x=0.15$, $x=0.30$, and $x=0.45$. As shown in the diagram, when the temperature is lowered from the DT state, the DT state is transformed into the OO state with CAF ordering, via a magnetically disordered OO state, for $0.10 \leqslant x < 0.25$ and into the ICOO state for $0.27 < x \leqslant 0.43$. In addition to these transitions, successive transitions take place from the DT state to the ICOO state, and then to the OO state, for $0.25 \leqslant x \leqslant 0.27$, while no transition occurs for $0.43 < x \leqslant 0.50$. Because the DT-to-ICOO transition is strongly suppressed for $x > 0.38$, the CECOO state never appears for $x=0.50$, unlike the case of SLMO.[14–20] As for the

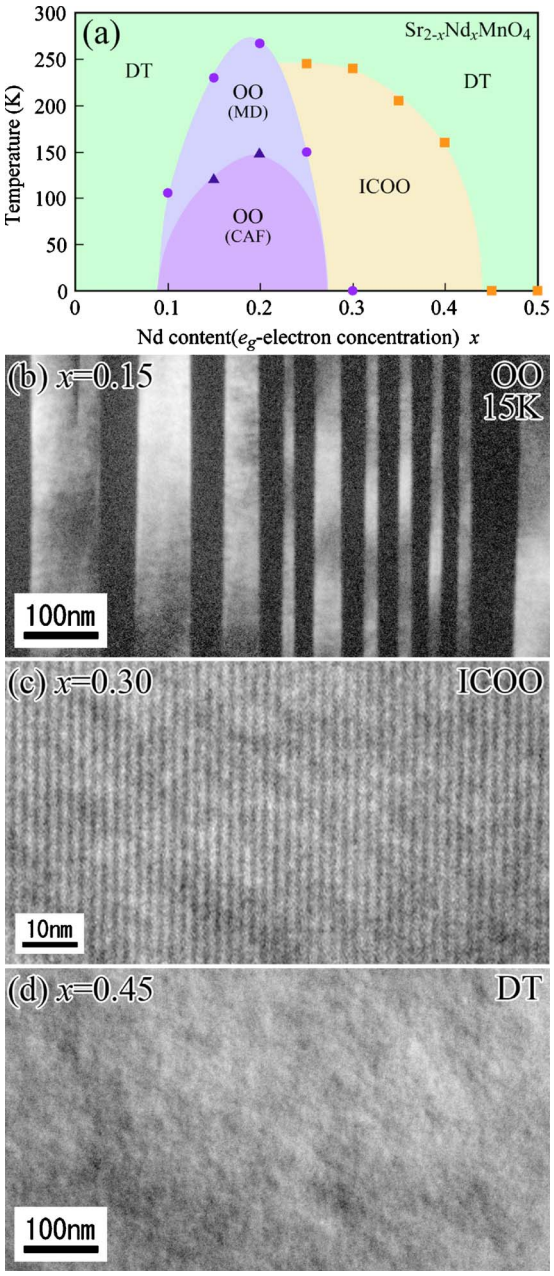

FIG. 1. (Color online) Sr-rich portion of the experimentally determined electronic phase diagram of $Sr_{2-x}Nd_xMnO_4$, together with dark field images of the OO (CAF), ICOO, and DT states at 15 K. In the diagram, the OO (CAF), OO (MD), ICOO, and DT states represent the orbital-ordered state accompanying the *C*-type antiferromagnetic (CAF) ordering, the orbital-ordered state with magnetic disordering (MD), the incommensurate charge-and-orbital-ordered state, and the disordered tetragonal state, respectively. The images in (b), (c), and (c) were, respectively, taken by using the 660 reflection for $x=0.15$, the 200 and surrounding satellite reflections for $x=0.30$, and the 200 reflection for $x=0.45$, in the [001] electron incidence.

microstructures of these electronic states, image (b) of the $x=0.15$ sample exhibits a banded domain structure indicating an alternating array of O_{I} and O_{II} bands with different b/a values in the OO state. As in image (c), fringes with a spacing of about $6.67d_{110}$, basically pointing to an incommensu-

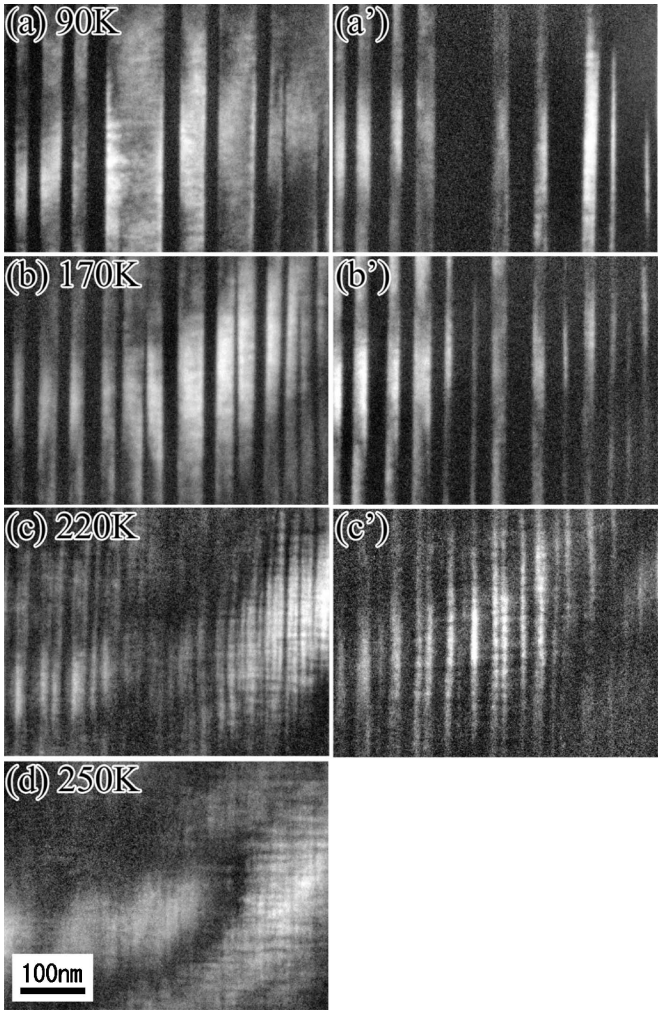

FIG. 2. A series of dark field images indicating the domain-structure evolution during the heating process for $x=0.15$. The sample heating resulted in the reverse successive transitions from the OO state with the CAF ordering to the OO state without magnetic ordering, and then to the DT state. The electron beam incidence for all images was parallel to the [001] direction.

rate modulation, are arranged along the [110] direction in the ICOO state. Note that d_{110} is the interplanar distance of the (110) plane in the DT state. Furthermore, in spite of the detection of a dotted contrast, no notable contrast, such as a tweed pattern, is evident in image (d) of the DT state.

At this point, we turn to a detailed description of the features of the domain-structure change during the transition between the DT and OO states. Figure 2 shows a series of dark field images indicating an OO-to-DT reverse transition during the heating process from 15 K. These images were obtained from the $x=0.15$ sample at 90 K for (a) and (a′), 170 K for (b) and (b′), 220 K for (c) and (c′), and 250 K for (d). In the figure, images (a), (b), and (c) on the left side were taken using the 660 reflection due to the O_{II} variant, while the 660 reflection due to the O_I variant was used for the images (a′), (b′), and (c′) on the right side. Image (d) was also obtained using the 660 reflection of the DT state. Note that, because the domain-structure relaxation occurred in this transition, each image was taken after the sample had been

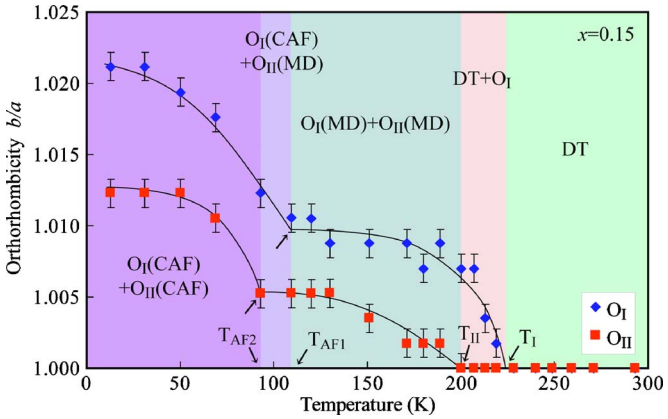

FIG. 3. (Color online) Variation of the b/a values for two OO variants, O_I and O_{II}, with orthorhombic symmetry as a function of temperature for $x=0.15$.

kept at an annealing temperature for more than 1 h. In addition, the notable change in the domain structures was found to take place mainly above 90 K. Only a few thin bands appeared between 15 and 90 K. Because of this, in Fig. 2, we show the images obtained in the temperature range above 90 K.

The banded domain structure with the (110) boundary at 90 K is shown in image (a) and (a′). As mentioned above, the banded structure in the OO state was not a usual O twin structure but consisted of an alternating array of O_I and O_{II} bands with different b/a values. When the temperature was raised from 90 K, new thin O_I and O_{II} bands appeared in the OO state, as seen in images (b) and (b′) at 170 K. This result implies that, in the OO state, the band density, defined as the number of bands per unit length, increases with rising temperatures. That is, the band density of the (O_I+O_{II}) banded structure seems to depend on the annealing temperature. From images (c) and (c′) at 220 K, we noted that a further heating resulted in the conversion of the O_{II} bands into DT bands. A feature of the images at 220 K is that the tweed-pattern contrast is evident in the DT bands; that is, the DT and OO states coexist at around 230 K for $x=0.15$. In image (d) at 250 K, after the reverse transition, we can finally detect only the tweed-pattern contrast, a finding suggesting the presence of JT clusters over an entire area of the sample.

In this study, the b/a values of the O_I and O_{II} bands at each temperature in the heating process were evaluated from the locations of the 660 reflections due to the O_I and O_{II} variants in the electron diffraction pattern. The determined values in the $x=0.15$ sample, kept at each temperature for more than 1 h, are plotted as a function of temperature in Fig. 3. The b/a values of the O_I and O_{II} variants at 15 K, as a starting state, were found to be 1.021 and 1.013, respectively. An increase in temperature led to a decrease in the b/a values for the O_I and O_{II} variants, which became zero at about 225 K, T_I, for the O_I and at about 200 K, T_{II}, for the O_{II}. The most striking feature of the change in the b/a value is that an anomaly occurs in both curves for the O_I and O_{II} variants, as indicated by the arrows. The temperatures at the anomaly were about 110 K for the O_I and about 90 K for the O_{II}. As for the origin of the anomaly in the b/a value,

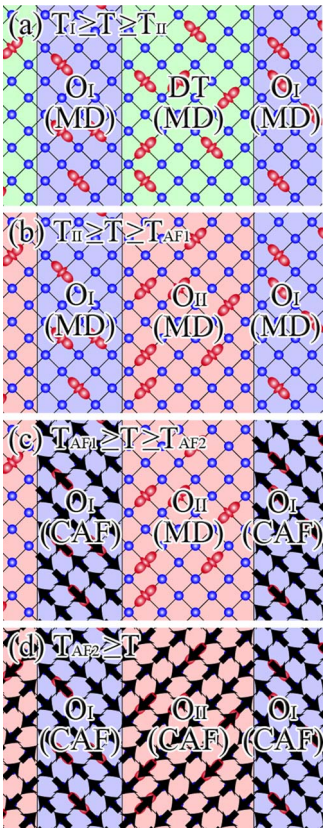

FIG. 4. (Color online) Schematic diagrams of the four banded-domain-structure states present in the OO state: (a) $T_I \geq T \geq T_{II}$, (b) $T_{II} \geq T \geq T_{AF1}$, (a) $T_{AF1} \geq T \geq T_{AF2}$, and (a) $T_{AF2} \geq T$. Because e_g electrons can hop between Mn sites along the orbital-elongated directions, these schematic diagrams should be snapshots of the four banded-domain-structure states. In the O_I(CAF) and O_{II}(CAF) bands, further, each thick arrow represents a direction of a local magnetic moment in a Mn site.

Kimura *et al.* have already found that a CAF ordering in SNMO accompanies an abrupt change in the a and b lattice parameters of the O lattice.[9] This earlier result is indicative of the fact that the CAF ordering appears at about 110 K, T_{AF1} for the O_I band and at about 90 K, T_{AF2}, for the O_{II} band.

The change in the b/a values of the O_I and O_{II} bands clearly attests that, in the OO state of SNMO, there exist four unique states characterized by banded domain structures. These four banded-domain-structure states are depicted in Fig. 4. The (DT+O_I) coexistence state lacking magnetic ordering is present in (a) $T_I \geq T \geq T_{II}$ as the highest-temperature region of the OO state. When the temperature is lowered in the OO state, the conversion of DT bands into O_{II} bands results in the (O_I+O_{II}) state without magnetic ordering for (b) $T_{II} \geq T \geq T_{AFI}$. These states in SNMO were also found in the OO state of SLMO.[19,20] The distinguishing mark of the OO state in SNMO is thus the appearance of the following two states with the CAF ordering. Concretely, the state for (c) $T_{AF1} \geq T \geq T_{AF2}$ consists of a quasiperiodic array of the O_I and O_{II} bands, and only the O_I bands accompany the CAF ordering. The ground OO state is then understood to be the (O_I+O_{II}) banded-structure state having different b/a values and different transition temperatures for the CAF ordering.

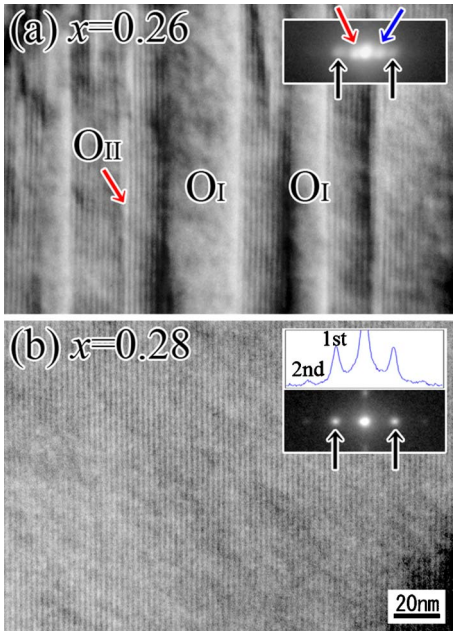

FIG. 5. (Color online) Dark field images indicating the ICOO state at 15 K for x=(a) 0.26 and (b) 0.28 near the OO (CAF)/ICOO phase boundary, together with corresponding electron diffraction patterns only around the 440 position. These two images were taken using the 220 and surrounding satellite reflections. The intensity profile through the 220 position along the $[1\bar{1}0]$ direction in the inset for x=0.28 clearly indicates the presence of the second-order satellite reflections suggesting a sinusoidal modulation. In the pattern for x=0.26, the black, blue, and red arrows indicate the first-order satellite reflections due to the ICOO state and the 440 reflections of the O_I and O_{II} variants in the OO state, respectively.

The ICOO state in SNMO is characterized mainly by the presence of incommensurate and higher-order commensurate structural modulations. Note that, before our study, only two commensurate modulations with even-integer periodicities of $6d_{110}$ and $8d_{110}$ were found in SNMO.[10] Figure 5 shows two dark field images of the ICOO state at 15 K near the OO/ICOO boundary in the phase diagram of Fig. 1(a). The images were actually taken from SNMO samples with x=0.26 and 0.28, together with corresponding electron diffraction patterns around the 440 position. We note both fringe-contrast regions, indicating the ICOO state, and O_I and O_{II} bands in the OO state in image (a) for x=0.26, that is, this sample at 15 K consists of the (ICOO+OO) coexistence state. On the basis of the average spacing between two neighboring fringes, the modulation in the fringe-contrast regions was determined to have a periodicity of about $7.70d_{110}$. In the diffraction pattern, furthermore, there are the first-order satellite reflections due to the modulation and the 440 reflections due to the O_I and O_{II} variants. The important feature is that, as indicated by the arrows, the locations of the 440 reflections due to the O_I and O_{II} variants are asymmetric with respect to the 440 position of the DT state, a situation corresponding to different b/a values. From these locations, we estimated the b/a values of the O_I and O_{II} variants to be about 1.013 and about 1.005, respectively; in that case, the

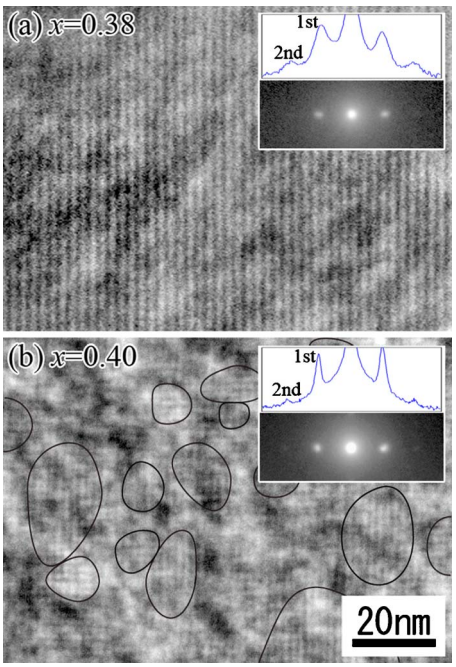

FIG. 6. (Color online) Dark field images and corresponding electron diffraction patterns around the 440 position, indicating the ICOO state at 15 K for x=(a) 0.38 and (b) 0.40 near the ICOO/DT phase boundary. These two images were taken using the 200 and surrounding satellite reflections. In the insets, the second-order reflections are clearly detected in the intensity profiles through the 440 position along the $[1\bar{1}0]$ direction. In the image for x=0.40, the black curves are just guides to the eyes for the boundaries of round-shaped domains distributed in the DT matrix.

CAF ordering should occur only in the O_I bands. On the other hand, in image (b) for the x=0.28 sample, we clearly see uniform fringes with an average spacing of about $7.14d_{110}$. The second-order satellite reflection indicating a sinusoidal modulation is also present in the diffraction pattern. Note that the second-order reflection was not detected in the x=0.26 sample.

As shown in the electronic phase diagram of Fig. 1(a), the stability of the ICOO state is strongly suppressed for $x>0.38$. To understand the characteristics of the suppression, the crystallographic features of the ICOO state near the ICOO/DT boundary were examined by transmission electron microscopy. Figure 6 shows both the dark field images and the corresponding electron diffraction patterns, indicating the ICOO state, of the x=0.38 and 0.40 samples at 15 K. The image in the x=0.38 sample exhibits uniform fringes with a determined periodicity of about $5.24d_{110}$, and the second-order reflections as well as the first-order reflections exist in the pattern, suggesting a sinusoidal modulation. In the x=0.40 sample, on the other hand, the ICOO state is found to consist of small round-shaped domains with an average size of about 20 nm, which are separated by disordered regions. The notable features of these nanometer-sized domains are that they basically have the same incommensurate periodicity, about $5.24d_{110}$, and that a certain phase shift between two neighboring domains occurs in a disordered region. Furthermore, in order to confirm the presence of such domains in the ICOO state, we examined the crystallographic features of other samples near the ICOO/DT phase boundary and found the same round-shaped domains for $0.38<x\leqslant 0.43$. The striking feature of such a domain is that a size of an individual domain tends to decrease with increments in the Nd content. In other words, the annihilation of the ICOO state occurred around x=0.43 via the decrease in the domain size in the (ICOO+DT) coexistence state.

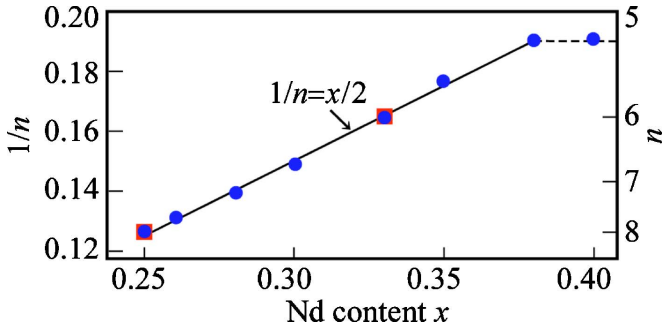

FIG. 7. (Color online) Nd-content dependence of an inverse periodicity $1/n$ for the structural modulation in the ICOO state. The inverse values for x=0.25 and 0.33, obtained by Nagai *et al.* (Ref. 10), are also plotted as the red squares in the figure.

Figure 7 shows the determined periodicity n of the modulation in each sample with the ICOO state. It should be remarked that, because the periodicity is independent of temperature in the entire ICOO state, the n values measured at various temperatures are plotted in the figure. As indicated in the figure, the inverse of the periodicity $1/n$ increases with increments in the Nd content where $0.25\leqslant x\leqslant 0.38$ and becomes an almost constant value for $0.38<x\leqslant 0.43$. The linear relation between $1/n$ and x in the former is confirmed, just as in the SLMO case, and is expressed by $1/n=x/2$.[14–20] On the other hand, the constant value in the latter higher Nd content region corresponds to an incommensurate periodicity of $n=5.24d_{110}$. In addition, the comparison with dark field images indicates that round-shaped domains in the ICOO state appear in the constant-periodicity region of $0.38<x\leqslant 0.43$. Because no change occurs in the periodicity, it is suggested that an increase in the e_g-electron concentration per unit periodicity should occur in the $0.38\leqslant x\leqslant 0.43$ region.

IV. DISCUSSION

The present TEM observations of SNMO revealed that, in the OO state, there existed four banded-domain-structure states, including the (DT+O_I) coexistence state, and that incommensurate and higher-order commensurate modulations occurred in the ICOO state. Another interesting feature is that round-shaped domains appeared in the ICOO state near the ICOO/DT phase boundary, a finding suggestive of the presence of the (ICOO+DT) coexistence state. On the basis of these results, we now discuss the origin of the appearance of these four banded-structure states in the OO state and propose an orbital-occupation model of the OO-to-ICOO ground-state change as a function of the e_g-electron concentration.

We start with a discussion of the appearance of the four banded-structure states in the OO state. It is understood that the DT-to-OO transition is characterized by the e_g-electron occupation of the $(3x^2-r^2)$ or $(3y^2-r^2)$ orbital. The corresponding structural order parameters in the transition can be identified as local JT distortions, which are associated with the two-dimensional E_g irreducible representation of the O_h group in the Koster notation.[21] In the D_{4h} group of the DT state, however, this representation is a reducible representation; it then reduces to the A_{1g} and B_{1g} representations. This implies that the local JT distortions should be coupled to two types of long-range distortions: the dilational distortion of $(e_{xx}+e_{yy})$ and the O distortion of $(e_{xx}-e_{yy})$ in the MnO_2 layer. Here, the following point should be remarked. Dilational distortion, when induced by the presence of an OO region, yields an expanded area that produces a contracted area around it. In the contracted area, the development of a ferro-orbital correlation among JT clusters is strongly suppressed. It is thus suggested that the appearance of the (DT $+O_{\mathrm{I}}$) coexistence state arises from a coupling between the local JT and the long-range dilational distortions. In other words, surprisingly, the structural order parameter associated with the reducible representation seems to be a key factor for the behavior of the DT-to-OO transition.

In addition to the $[\mathrm{DT}+O_{\mathrm{I}}(\mathrm{MD})]$ and $[O_{\mathrm{I}}(\mathrm{MD})+O_{\mathrm{II}}(\mathrm{MD})]$ banded-structure states, it was found that, in the OO state of SNMO, there are two more states with the $[O_{\mathrm{I}}(\mathrm{CAF})+O_{\mathrm{II}}(\mathrm{MD})]$ and $[O_{\mathrm{I}}(\mathrm{CAF})+O_{\mathrm{II}}(\mathrm{CAF})]$ banded structures, where MD denotes magnetic disordering. That is, the latter states accompany the CAF ordering. It is obvious that orbital ordering without charge ordering facilitates the appearance of CAF ordering with parallel spins along the orbital-elongated direction. It does so because the strong transfer interaction of the e_g electrons along the [100] direction can, for instance, be stabilized by the $(3x^2-r^2)$ orbital. If we accept the fact that CAF ordering occurs in SNMO, then the appearance of the two states with that ordering results from the difference in the transition temperature of the CAF ordering between the O_{I} and O_{II} bands. As for the difference in the transition temperature, the experimental data in Fig. 3 clearly indicate that the transition temperature of the CAF ordering depends on the b/a value, that is, orthorhombicity, reflecting a degree of orbital ordering. Because the long-range distortion involves the two contributions of the dilational A_{1g} and orthorhombic B_{1g} distortions, as was mentioned above, the b/a value must be controlled by the spatial distributions of the A_{1g} and B_{1g} distortions. In other words, it is suggested that the transition temperature of the CAF ordering is directly associated with the interaction between these two long-range distortions. In this scenario, the dilational distortion may also play an essential role in the appearance of the two low-temperature states with the CAF ordering, in addition to the $(\mathrm{DT}+O_{\mathrm{I}})$ coexistence state.

The ICOO state in SNMO was found to exist for $0.25 \leqslant x \leqslant 0.43$. Because the relation between the periodicity n and the Nd content x is expressed by $n=2/x$, the ICOO state must be basically characterized by incommensurate structural modulations. The important feature to note here is that the structural modulation can be identified as a sinusoidal transverse-displacement wave on the basis of both the presence of the second-order satellite reflection and the extinction rule of satellite reflections. In other words, because the point group of the [110] symmetry line in the DT state is the C_{2v} group, the transition to the ICOO state is associated with the Σ_4 irreducible representation in the Koster notation.[21] Thus, an incommensurate displacement wave ϕ with $q\|[\zeta\zeta 0]$ and $e\|[1\bar{1}0]$ and a corresponding distortion wave given by $\Phi=d\phi/dr$ are depicted in Fig. 8 for the ζ value corresponding to $n=6.7d_{110}$. These diagrams tell us that the

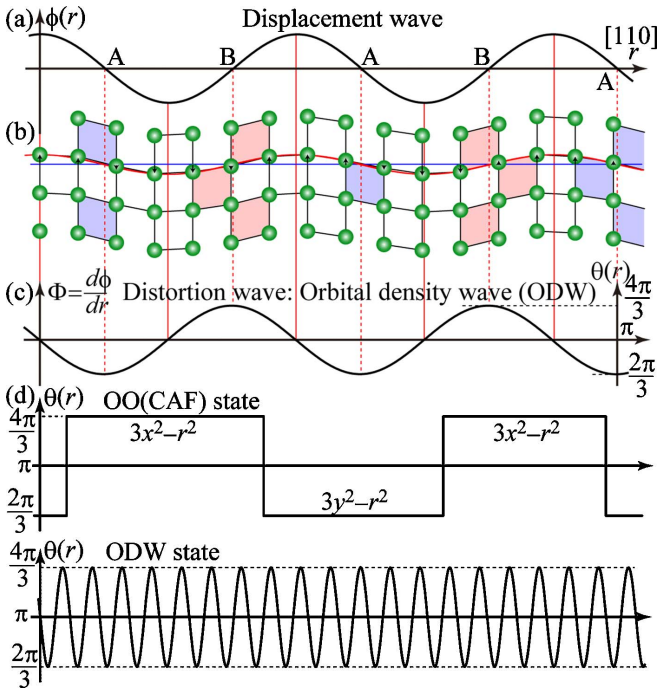

FIG. 8. (Color online) Schematic diagrams of the displacement and distortion waves for the structural modulation with the incommensurate periodicity of $6.7d_{110}$ in the ICOO state. Based on the fact that the satellite reflections in the diffraction patterns disappear for a scattering vector parallel to a wave vector q of the modulation, the displacement wave in (a) can basically be identified as a transverse wave ϕ with $q\|[\zeta\zeta 0]$ and $e\|[1\bar{1}0]$. As for atomic shifts in the displacement wave, since our interest is focused on a structural response to the orbital density wave (ODW), only the oxygen positions represented by the green circles are depicted in (b). Note that the oxygen-ion displacements in this diagram are exaggerated for clarity. The feature of the obtained positions is that a square shape consisting of four oxygen ions is deformed into a rhombic shape around the nodes of the displacement wave. Because the oxygen positions with a rhombic shape should reflect a structural response to the ODW, the distortion wave $\Phi=d\phi/dr$ as a direct response is shown in (c). In order to clearly indicate the correspondence between the distortion wave and the ODW, the θ axis is added in the right side of (c). Based on this correspondence, the spatial variation of the θ value for the OO(CAF) and ICOO states is then depicted in (d). When the O_{I} and O_{II} bands are, respectively, assumed to have the θ values of $4\pi/3$ and $2\pi/3$, the OO state can be expressed as a square θ wave. On the other hand, the θ value in the ICOO state continuously changes between $4\pi/3$ and $2\pi/3$. That is, the ICOO state can be regarded as a modulated-structure state of the OO state with respect to the θ value.

$(3x^2-r^2)$- and $(3y^2-r^2)$-like orbital orderings should occur, respectively, around the two types of nodes specified by letters the A and B. That is, the distortion wave Φ is a structural response to the orbital ordering, and Φ^2 would reflect the e_g-electron density. Here, it should be remarked that Nagai *et al.* already found the presence of the ICOO state, including incommensurate modulations, in $Ca_{2-x}Nd_xMnO_4$ and proposed a charge-orbital density wave as a model of the state.[22] According to their model, the orbital density wave (ODW) can be expressed as $|d(\theta)\rangle=\cos(\theta/2)|d_{3z^2-r^2}\rangle+\sin(\theta/2)|d_{x^2-y^2}\rangle$, where θ is a function of the position and $|d_{3z^2-r^2}\rangle=(1/\sqrt{6})(2z^2-x^2-y^2)$ and $|d_{x^2-y^2}\rangle=(1/\sqrt{2})(x^2-y^2)$. The values of $\theta=2\pi/3$, π, and $4\pi/3$ correspond to the $(3y^2-r^2)$, (x^2-y^2), and $(3x^2-r^2)$ orbital states, respectively, and the ODW can be characterized by the θ range of $2\pi/3 \leqslant \theta \leqslant 4\pi/3$. We believe that, because the distortion wave is sinusoidal, their model must be appropriate for the ICOO state in SNMO. In other words, the distortion wave should be a direct structural response to the sinusoidal ODW, as shown in Fig. 8(c). It is thus likely that the ICOO state in SNMO is mainly characterized by the sinusoidal ODW, whose structural response is the distortion wave derived from the sinusoidal displacement wave found experimentally. In addition, a charge density modulation may occur as a charge density wave (CDW) in the ODW state, because Φ^2 would reflect the e_g-electron density. As the ODW model allows disordering for the site occupation of e_g electrons, further, the increase in the e_g-electron concentration per a unit periodicity for $0.38 \leqslant x \leqslant 0.43$ can be easily explained as an increase in the amplitude of the CDW.

When the e_g-electron concentration increases in SNMO, the ground state changes from the OO(CAF) state to the ODW state at around $x=0.25$. In the ODW model, as mentioned above, the ICOO state is characterized by the θ range of $2\pi/3 \leqslant \theta \leqslant 4\pi/3$, while $\theta=2\pi/3$ and $4\pi/3$ correspond to two variants in the OO(CAF) state. This indicates that the OO(CAF)-to-ICOO ground-state change can be expressed as $(\theta=2\pi/3$ or $4\pi/3) \rightarrow (2\pi/3 \leqslant \theta \leqslant 4\pi/3)$ with respect to the θ value. Figure 8(d) depicts one-dimensional schematic diagrams of the OO(CAF) and ICOO states as a function of the position. In the diagram, a vertical axis represents the θ value, and the O_{I} and O_{II} variants are assumed to have the θ values of $4\pi/3$ and $2\pi/3$, respectively. As easily understood from the diagrams, the ICOO state characterized by the sinusoidal ODW is just a modulated-structure state of the OO state with respect to the θ value. Based on the connection between the orbital-ordered characteristics of the OO and ICOO states, it seems to us that the OO-to-ICOO ground-state change is a natural consequence for an increase in the e_g-electron concentration in the two-dimensional electron system.

We finally compare the ODW model for the ICOO state with that proposed by Kimura *et al.*[9] In their model, the ICOO state in SNMO, consisting of only two commensurate modulations, is characterized by a zigzag ferromagnetic chain. The short ferromagnetic chain arises from the orbital ordering of the alternate $(3x^2-r^2)/(3y^2-r^2)$. The state in their model then consists of an alternating array of two nanometer-sized bands with $(3x^2-r^2)$ and $(3y^2-r^2)$ orbital orderings. In other words, their ODW model is based on a square-wave modulation with a nanometer-sized wavelength. Because the square ODW should result in a square distortion wave as a structural response, the difference between the OO and square ICOO states is only a width for the O_{I} and O_{II} bands. It is, however, obvious that the square ODW is not compatible with the sinusoidal displacement wave found in this study. Apparently, thus, the disagreement may rule out the square ODW picture for the ICOO state in SNMO.

V. CONCLUSIONS

In the layered perovskite SNMO, the OO state exists for $0.10 \leqslant x \leqslant 0.27$ and ICOO state for $0.25 \leqslant x \leqslant 0.43$. An interesting feature of the appearance of these states in the phase diagram is that the DT state surrounds the region where the OO and ICOO states are present. Based on this feature, we believe that the electronic state in the ICOO state should be related to that in the OO state. For these two states, we should note the following details: the OO state consists of the four banded-structure states including the $(\mathrm{DT}+O_{\mathrm{I}})$ coexistence state, and the ground state of the OO state is likely to be the $(O_{\mathrm{I}}+O_{\mathrm{II}})$ banded-structure state with CAF ordering. On the other hand, the ICOO state can be characterized by a sinusoidal transverse-displacement modulation, and the (ICOO+DT)) coexistence state is present for $0.38 < x \leqslant 0.43$. Because the relation between the periodicity n and the Nd content x is expressed by $n=2/x$ in the region of $0.25 \leqslant x \leqslant 0.38$, the modulation is basically incommensurate. Here, the point to note is that the sinusoidal, incommensurate modulation should lead to a sinusoidal distortion wave as a direct structural response to the orbital ordering in the ICOO state. It is likely that the sinusoidal ODW accompanying the charge density modulation is the most appropriate model for the ICOO state. In this model, the ICOO state is a modulated-structure state of the OO state with respect to the θ value. It is thus understood that the OO-to-ICOO ground-state change, which is produced by an increase in the e_g-electron concentration, should be associated with the introduction of a modulated θ wave into the OO state.

*wataru@ruri.waseda.jp

[1] S. Jin, T. H. Tiefel, M. McCormack, R. A. Fastnacht, R. Ramesh, and L. H. Chen, Science **264**, 413 (1994).
[2] Y. Tokura, A. Urushibara, Y. Moritomo, T. Arima, A. Asamitsu, G. Kido, and N. Furukawa, J. Phys. Soc. Jpn. **63**, 3931 (1994).
[3] G. C. Xiong, Q. Li, H. L. Ju, S. N. Mao, L. Senapati, X. X. Xi, R. L. Greene, and T. Venkatesan, Appl. Phys. Lett. **66**, 1427 (1995).
[4] E. Dagotto, T. Hotta, and A. Moreo, Phys. Rep. **344**, 1 (2001).
[5] J. Burgy, M. Mayr, V. Martin-Mayor, A. Moreo, and E. Dagotto,

Phys. Rev. Lett. **87**, 277202 (2001).
[6] K. H. Ahn, T. Lookman, and A. R. Bishop, Nature (London) **428**, 401 (2004).
[7] T. Lookman, S. R. Shenoy, K. O. Rasmussen, A. Saxena, and A. R. Bishop, Phys. Rev. B **67**, 024114 (2003).
[8] Y. Yamada and T. Takakura, J. Phys. Soc. Jpn. **71**, 2480 (2002).
[9] T. Kimura, K. Hatsuda, Y. Ueno, R. Kajimoto, H. Mochizuki, H. Yoshizawa, T. Nagai, Y. Matsui, A. Yamazaki, and Y. Tokura, Phys. Rev. B **65**, 020407(R) (2001).
[10] T. Nagai, T. Kimura, A. Yamazaki, T. Asaka, K. Kimoto, Y. Tokura, and Y. Matsui, Phys. Rev. B **65**, 060405(R) (2002).
[11] M. Daghofer, A. Oles, D. Neuber, and W. von der Linden, Phys. Rev. B **73**, 104451 (2006).
[12] J. Bouloux, J. Soubeyroux, G. Flem, and P. Hagenguller, J. Solid State Chem. **38**, 34 (1981).
[13] W. Norimatsu and Y. Koyama, Physica C (to be published).
[14] Y. Moritomo, Y. Tomioka, A. Asamitsu, Y. Tokura, and Y. Matsui, Phys. Rev. B **51**, 3297 (1995).
[15] W. Bao, C. H. Chen, S. A. Carter, and S.-W. Cheong, Solid State Commun. **98**, 55 (1996).
[16] S. Larochelle, A. Mehta, N. Kaneko, P. K. Mang, A. F. Panchula, L. Zhou, J. Arthur, and M. Greven, Phys. Rev. Lett. **87**, 095502 (2001).
[17] S. Larochelle, A. Mehta, L. Lu, P. K. Mang, O. P. Vajk, N. Kaneko, J. W. Lynn, L. Zhou, and M. Greven, Phys. Rev. B **71**, 024435 (2005).
[18] Y. Moritomo, A. Nakamura, S. Mori, N. Yamamoto, K. Ohoyama, and M. Ohashi, Phys. Rev. B **56**, 14879 (1997).
[19] W. Norimatsu and Y. Koyama, Phys. Rev. B **74**, 085113 (2006).
[20] W. Norimatsu and Y. Koyama, Phys. Rev. B **75**, 104416 (2007).
[21] G. F. Koster, *Solid State Physics*, edited by F. Seitz and D. Turnbull (Academic, New York, 1957), Vol. V.
[22] T. Nagai, T. Kimura, A. Yamazaki, Y. Tomioka, K. Kimoto, Y. Tokura, and Y. Matsui, Phys. Rev. B **68**, 092405(R) (2003).